https://doi.org/10.1093/plphys/kiad084 PLANT PHYSIOLOGY 2023: 192: 370–386

Plant Physiology®

Research Article

High cyclic electron transfer via the PGR5 pathway in the absence of photosynthetic control

Gustaf E. Degen [1], Philip J. Jackson [1,2], Matthew S. Proctor [1], Nicholas Zoulias [1], Stuart A. Casson [1] and Matthew P. Johnson [1,*]

1 Plants, Photosynthesis and Soil, School of Biosciences, University of Sheffield, Firth Court, Western Bank, Sheffield S10 2TN, UK
2 Department of Chemical and Biological Engineering, University of Sheffield, Sheffield S1 4NL, UK

*Author for correspondence: matt.johnson@sheffield.ac.uk
The author responsible for distribution of materials integral to the findings presented in this article in accordance with the policy described in the Instructions for Authors (https://academic.oup.com/plphys/pages/General-Instructions) is Matthew P. Johnson.

Abstract

The light reactions of photosynthesis couple electron and proton transfers across the thylakoid membrane, generating NADPH, and proton motive force (pmf) that powers the endergonic synthesis of ATP by ATP synthase. ATP and NADPH are required for CO_2 fixation into carbohydrates by the Calvin–Benson–Bassham cycle. The dominant ΔpH component of the pmf also plays a photoprotective role in regulating photosystem II light harvesting efficiency through nonphotochemical quenching (NPQ) and photosynthetic control via electron transfer from cytochrome b_6f (cytb_6f) to photosystem I. ΔpH can be adjusted by increasing the proton influx into the thylakoid lumen via upregulation of cyclic electron transfer (CET) or decreasing proton efflux via downregulation of ATP synthase conductivity (gH^+). The interplay and relative contributions of these two elements of ΔpH control to photoprotection are not well understood. Here, we showed that an Arabidopsis (*Arabidopsis thaliana*) ATP synthase mutant *hunger for oxygen in photosynthetic transfer reaction 2* (*hope2*) with 40% higher proton efflux has supercharged CET. Double crosses of *hope2* with the CET-deficient *proton gradient regulation* 5 and *ndh-like photosynthetic complex I* lines revealed that PROTON GRADIENT REGULATION 5 (PGR5)-dependent CET is the major pathway contributing to higher proton influx. PGR5-dependent CET allowed *hope2* to maintain wild-type levels of ΔpH, CO_2 fixation and NPQ, however photosynthetic control remained absent and PSI was prone to photoinhibition. Therefore, high CET in the absence of ATP synthase regulation is insufficient for PSI photoprotection.

Introduction

CO_2 fixation into biomass during photosynthesis requires reducing power in the form of NADPH and energy in the form of ATP (Kramer and Evans 2011). NADPH is provided by coupled photosynthetic linear electron transfer (LET) reactions in the thylakoid membrane, which also generate pmf for ATP synthesis via ATP synthase. In chloroplasts, proton motive force (pmf) is largely composed of the proton concentration gradient (ΔpH), with minimal contribution from the membrane potential ($\Delta\Psi$) in the steady-state (Wilson et al. 2021), which is detrimental to productive charge separation in photosystem II (PSII) (Davis et al. 2016) and largely dissipated by counterion movements (Hind et al. 1974). In addition to its manifest role in ATP synthesis, the ΔpH also plays a vital role in regulating photosynthetic electron transfer and light harvesting reactions via photosynthetic control and energy-dependent nonphotochemical quenching (NPQ), known as qE (Li et al. 2009; Malone et al. 2021). Photosynthetic control restricts the rate of plastoquinol (PQH_2) oxidation at cytb_6f activity, can be measured as the donor-side limitation of photosystem I (PSI) (Y(ND)) using P700 absorption spectroscopy and protects PSI against photo-oxidative damage in excess light (Jahns et al. 2002; Suorsa et al. 2013). By contrast, qE involves ΔpH-induced protonation of the PsbS protein and de-epoxidation of the light harvesting antenna complex II (LHCII)-bound xanthophyll violaxanthin to zeaxanthin, which collectively bring

Received September 25, 2022. Accepted January 24, 2023. Advance access publication February 12, 2023
© American Society of Plant Biologists 2023. All rights reserved. For permissions, please e-mail: journals.permissions@oup.com

about energy dissipation in LHCII, protecting PSII from photo-oxidative damage (Ruban et al. 2012). qE can be measured as the rapidly-relaxing component of NPQ using pulse-amplitude modulated chlorophyll fluorescence. These ΔpH-dependent regulatory mechanisms are critical to plant growth in fluctuating light environments and rely on the careful modulation of the proton influx/efflux reactions across the thylakoid membrane (Armbruster et al. 2017).

Proton efflux is regulated primarily by the conductivity (gH^+) and abundance of the chloroplast ATP synthase (Kramer et al. 2004). Antisense mutants of the γ-subunit in *Nicotiana benthamiana* showed that ATP-synthase levels could be reduced by 50% without affecting gH^+ or pmf, while further decreases diminished gH^+ and increased pmf leading to higher qE and Y(ND) (Rott et al. 2011). Regulation of the ATP-synthase activity is therefore a key element of proton efflux control. Two types of regulation have been described for ATP synthase; redox and metabolic control (Mills and Mitchell 1982; Ort and Oxborough 1992; Kanazawa and Kramer 2002; Kohzuma et al. 2013). Redox control of ATP synthase is mediated by the reduction–oxidation status of two regulatory cysteines (C202 and C208 in *Arabidopsis thaliana*) which form a disulfide bridge stabilizing a loop of the γ1-subunit that acts as a chock, interfering with the rotation of the catalytic F1 head of the enzyme involved in ATP synthesis (Hisabori et al. 2003; Hahn et al. 2018). Therefore, a lower threshold pmf is required to activate the reduced enzyme (Junesch and Gräber 1987). Upon illumination, activation of LET causes reduction of ferredoxin (Fd) and NADPH, these can reduce thioredoxin (TRX) proteins via the Fd-dependent thioredoxin reductase (FTR) or NADPH dependent thioredoxin reductase (NTRC) enzymes. TRX then reduces the regulatory disulfide in the γ1-subunit (Carrillo et al. 2016; Sekiguchi et al. 2020). By contrast, inactivation of LET in the dark leads to gradual oxidation of the regulatory cysteines by 2-Cys peroxiredoxin, restoring the higher pmf threshold for activation (Ojeda et al. 2018). In addition to redox control, gH^+ is known to be modified by varying NADPH, CO_2, and Pi concentration suggesting ATP synthase is also under metabolic control (Kanazawa and Kramer 2002; Avenson et al. 2005; Takizawa et al. 2008; Kohzuma et al. 2013). Though the mechanism of metabolic control of ATP synthase remains to be elucidated. The *mothra* mutant of Arabidopsis has changes in three conserved acidic residues in the γ1-subunit (D211V, E212L, and E226L) resulting in the loss of redox sensitivity (Kohzuma et al. 2012). The pmf threshold for activation in *mothra* is correspondingly higher resulting in a lower gH^+, increased pmf, increased qE and lower LET rate, yet gH^+ varies with CO_2 concentrations, suggesting that metabolic control is unaffected. By contrast, in the Arabidopsis γ1-subunit mutant *hope2* (*hunger for oxygen in photosynthetic electron transport 2*, a G134D amino acid change in a putative NADP(H)-binding motif in the Rossman fold), renders gH^+ insensitive to changing CO_2 concentration, although redox control appears normal (Takagi et al. 2017). Interestingly, *hope2* showed a different phenotype to *mothra* with increased gH^+, the virtual absence of Y(ND), and a greater susceptibility to PSI photoinhibition, although maximum LET rate and CO_2 assimilation were unaffected. Crucially, the phenotype of *hope2* was successfully ameliorated via complementation with a wild type copy of the γ1-subunit.

Proton influx can occur via one of several coupled electron transfer pathways. LET involves the light-powered transfer of electrons from water to $NADP^+$, via a chain including PSII, plastoquinone (PQ)/PQH_2, cytb_6f, plastocyanin (Pc), PSI, Fd and ferredoxin-$NADP^+$ reductase (FNR). Unlike LET, alternative electron flows can contribute to pmf generation without generating net NADPH. These include; pseudo-cyclic electron transfer (CET, water-water cycle), where electrons from Fd are instead transferred to oxygen via flavodiiron (Flv) proteins to form water; the Mehler reaction, where PSI directly reduces oxygen to superoxide; and the malate valve, where NADPH is consumed to reduce oxaloacetate to malate, which can be exported from the chloroplast to be oxidized in the mitochondria (Miyake 2010; Alric and Johnson 2017). However, in angiosperms such as Arabidopsis, Flv proteins are absent and the primary alternative electron flow is CET, where electrons from Fd reduce PQ forming a cycle around PSI and cytb_6f via Fd–PQ reductase activity (FQR) (Johnson 2011; Yamori and Shikanai 2015). Two CET pathways occur in Arabidopsis, one sensitive to the inhibitor antimycin-A (AA) involves the PROTON GRADIENT REGULATION 5 (PGR5) protein (referred to as CET1) and the second is catalyzed by the NDH-like photosynthetic Complex I (NDH, referred to as CET2) (Yamori and Shikanai 2015). How PGR5 mediates CET1 remains unknown, early ideas that it acts together with PGR5-like photosynthetic phenotype 1 (PGRL1) to form an FQR (DalCorso et al. 2008; Hertle et al. 2013) were recently invalidated by evidence showing that PGRL1 channels PGR5 activity and protects PGR5 from degradation by PGR5-LIKE 2 (PGRL2) (Rühle et al. 2021). An alternative suggestion is that the cytb_6f complex binds FNR and together they play the role of the FQR (Shahak et al. 1981; Joliot and Johnson 2011). However while cytb_6f can be co-purified with FNR (Clark et al. 1984; Zhang et al. 2001), to date no FNR–cytb_6-f–PGR5 complex possessing the requisite FQR activity, which can be as high as 130 e^{-1} s^{-1} in Arabidopsis (Joliot et al. 2004), has been isolated. By contrast, high-resolution structures of the NDH–PSI CET2 supercomplex from Arabidopsis and barley (*Hordeum vulgare*) have been described (Shen et al. 2022; Su et al. 2022). The Arabidopsis *ndho* and *crr* mutants, which both lack NDH-dependent CET2, have relatively mild phenotypes with only slight differences seen in pmf generation and photosynthetic activity (Munekage et al. 2004; Wang et al. 2015; Nikkanen et al. 2018). On the other hand, the Arabidopsis *pgr5* mutant suffers a substantial loss of ΔpH, qE, and Y(ND) in high light together with lower LET, CO_2 assimilation, and increased PSI photoinhibition (Munekage et al. 2004; Suorsa et al. 2012; Nikkanen et al. 2018). The

more severe phenotype of *pgr5* suggests that CET1 is the dominant pathway in Arabidopsis and that NDH-dependent CET2 has a limited capacity to compensate. A number of high cyclic electron flow (*hcef*) mutants have been described in Arabidopsis and *N. benthamiana* (Livingston et al. 2010a, b; Strand et al. 2017). Yet to date, those *hcef* mutants characterized in detail have only shown upregulation of the NDH-dependent CET2 pathway (Livingston et al. 2010a, b; Strand et al. 2017), leading some to speculate that PGR5 may not be directly involved in CET (Suorsa et al. 2012; Takagi and Miyake 2018). Interestingly, *pgr5* also shows a high gH^+ phenotype, leading to the suggestion that it may alternatively regulate ATP synthase (Avenson et al. 2005). However, to date no interaction between these proteins has been observed. Moreover, overexpression of pseudo-CET inducing Flv proteins from *Physcomitrium* in the *pgr5* mutant was able to restore pmf to wild-type levels and ameliorated the high gH^+ phenotype, arguing against direct regulation of ATP synthase by PGR5 (Yamamoto et al. 2016). The low pmf in *pgr5* is also unlikely to be the cause of the high gH^+ since low pmf in the Arabidopsis *pgr1* mutant of cytb_6f was accompanied by contrastingly low gH^+ (Yamamoto and Shikanai 2020). Therefore, the cause of high gH^+ in *pgr5* remains unknown.

The fact that *hope2* and *pgr5* mutants share a low Y(ND), high gH^+ phenotype but differ in their respective capacities for qE, CO_2 assimilation, and LET (Munekage et al. 2004; Takagi et al. 2017) suggests that proton influx and efflux may play distinct roles in photosynthetic regulation. Here, we investigated these relationships further by creating double mutants lacking *hope2* and either *ndho* or *pgr5*. The results unexpectedly demonstrate that loss of ATP-synthase regulation in *hope2* is compensated for by increased PGR5-dependent CET, which maintains ΔpH and qE but fails to restore photosynthetic control.

Results

Hope2 maintains wild-type levels of pmf due to increased proton flux

We first sought to confirm that the CO_2 assimilation (A) phenotype of *hope2* was wild type-like as previously reported (Takagi et al. 2017). Indeed, A in *hope2* was similar to wild-type Col-0 at both high and low light intensity, although between 100 and 275 µmol photons m^{-2} s^{-1} A was slightly lower in *hope2* (Fig. 1A). The A/C_i response in *hope2* was not significantly different to the wild-type Col-0 (Fig. 1B). By contrast, in *pgr5* we find A in response to light and varying intercellular CO_2 concentrations (C_i) is lower compared to the wild-type *gl1* (Fig. 1, A and B). To estimate maximum Rubisco carboxylation rates in vivo ($V_{c,max}$) and maximum electron transport rate used in RuBP regeneration (J_{max}), we fit the Farquhar–von Caemmerer–Berry (FvCB) model (Farquhar et al. 1980) to individual A/C_i curves. $V_{c,max}$ and J_{max} were not different in *hope2* compared to Col-0 ($P > 0.05$), confirming that carbon fixation is not limited, in contrast to CET1-deficient *pgr5* ($P < 0.05$). This confirms that despite sharing the high gH^+ phenotype with *pgr5*, *hope2* is still able to maintain an optimal ATP/NADPH ratio for CO_2 assimilation.

We investigated how *hope2* is able to achieve wild type-like CO_2 assimilation further by comparing the generation of pmf in *hope2* and *pgr5* during photosynthetic induction. During the first 50 s of illumination, pmf in *hope2* was lower compared to *pgr5* and wild type (Fig. 1C), due to increased gH^+ levels (Fig. 1D), while proton flux (vH^+) was similar to *pgr5* and wild type (Fig. 1E). Thus, during the first 50 s of photosynthetic induction gH^+ regulation makes a larger contribution to pmf than vH^+. After 3 min, pmf in *hope2* reached wild-type levels, despite high gH^+, due to strongly increased vH^+ (Fig. 1, C–E). By contrast, pmf in *pgr5* dropped continuously during the first ∼200 s of actinic light exposure due to a combination of increasing gH^+ and low vH^+ (Fig. 1, C–E). Therefore, on longer timescales increases in vH^+ are important for maintaining pmf in the wild type as the gH^+ regulation relaxes. In *hope2*, the lack of gH^+ regulation leads to a compensatory increase in vH^+, maintaining pmf at wild-type levels beyond ∼150 s illumination. Having established that *hope2* had wild-type-level pmf after 6 min of low actinic light, we next investigated how *hope2* and *pgr5* behaved during increasing light intensities. This revealed that pmf in the wild-type plateaued at approximately 0.8 at 250 µmol photons m^{-2} s^{-1} (Fig. 1F), similar to previous reports (Nishikawa et al. 2012; Wang et al. 2015; Yamamoto et al. 2016; Nikkanen et al. 2018, 2019; Yamamoto and Shikanai 2020; Hepworth et al. 2021; Rühle et al. 2021) and pmf in *hope2* was not significantly different at all light intensities. gH^+ and vH^+ on the other hand, were still higher in *hope2* (Fig. 1, G and H), confirming that increased vH^+ drives the maintenance of wild-type levels of pmf in *hope2*. On the other hand, *pgr5* had diminished pmf at all but the lowest light intensity due to a combination of lower vH^+ and higher gH^+ compared to the wild type (Fig. 1, G and H).

Cyclic electron transfer is upregulated in hope2

We find that increased gH^+ in *hope2* is compensated for by an increase in vH^+, which could be caused by either increased LET, CET or another alternative electron flow. To test this further, we compared the thylakoid proteomes for proteins that were up or downregulated in *hope2* relative to the wild type (Supplemental Fig. S1). As expected, ATP-synthase abundance was decreased by ∼50% in *hope2* consistent with past immunoblotting results (Takagi et al. 2017). Other proteins significantly upregulated ($P < 0.05$) included the state transition kinases STN7 and STN8, PsbS, violaxanthin de-epoxidase, and the H^+/K^+ antiporter KEA3, while those downregulated included thioredoxin M2 (TRXM2), photosystem I subunit O (PSAO), and photosystem II reaction center protein T (PSBT). Most strikingly however, PGR5 (0.56-fold increase) and multiple subunits of the NDH complex (ndhF, H, I, K, M, N, O, S, and U) (∼0.21- to 0.41-fold

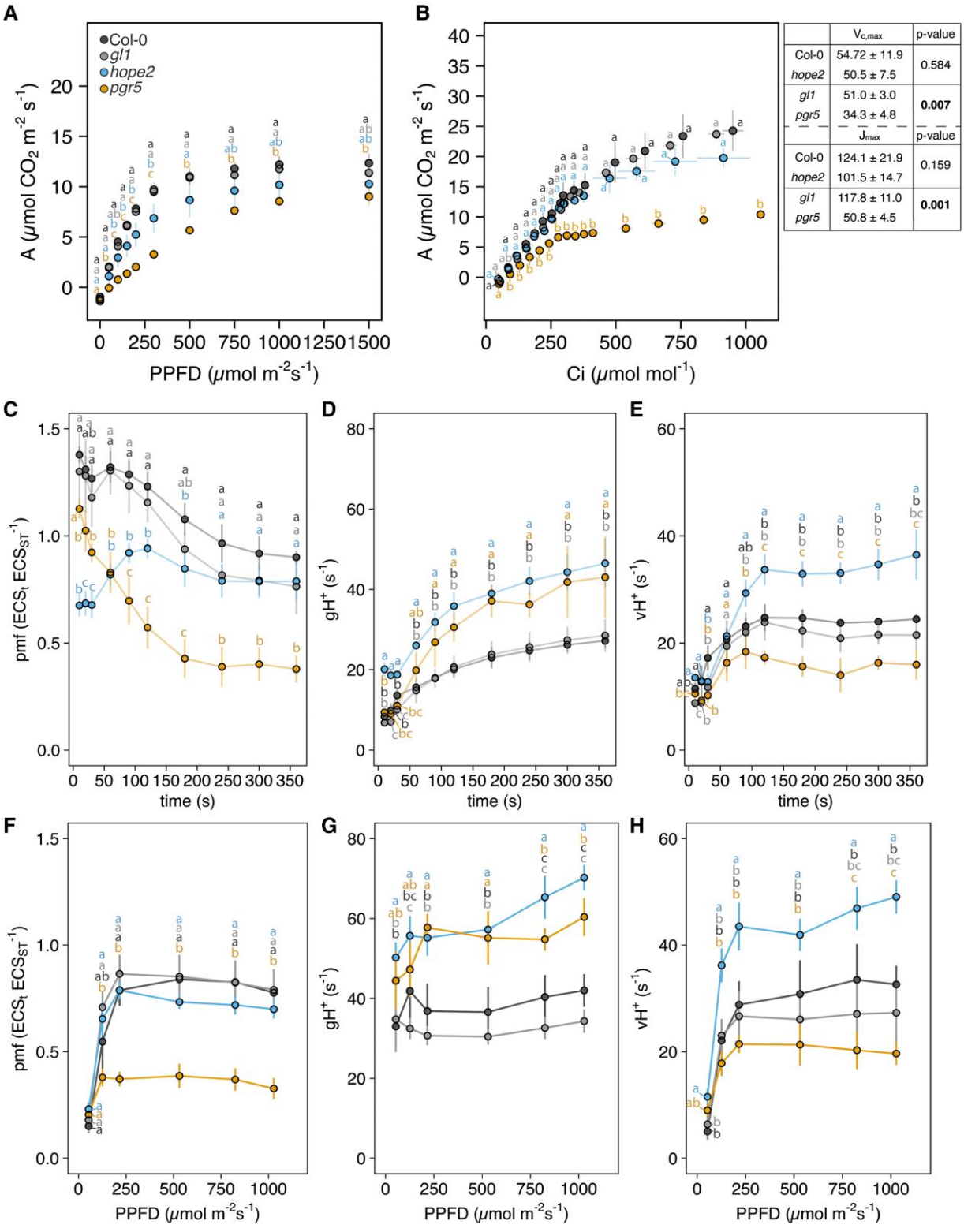

	$V_{c,max}$	p-value
Col-0	54.72 ± 11.9	0.584
hope2	50.5 ± 7.5	
gl1	51.0 ± 3.0	**0.007**
pgr5	34.3 ± 4.8	
	J_{max}	p-value
Col-0	124.1 ± 21.9	0.159
hope2	101.5 ± 14.7	
gl1	117.8 ± 11.0	**0.001**
pgr5	50.8 ± 4.5	

Figure 1. Gas-exchange and ECS measurements of wild type, *hope2* and *pgr5*. A) CO_2-assimilation at various light intensities. Plants were adapted to 400 ppm reference CO_2 and 1,500 µmol photons m^{-2} s^{-1} light for at least 10 min until steady-state was reached. Light levels were decreased stepwise, and data logged after at least 3 min at each light intensity. B) CO_2-assimilation at various C_i concentrations. Plants were adapted to 400 ppm reference CO_2 and 1,500 µmol photons m^{-2} s^{-1} light for at least 10 min until steady-state was reached. Reference CO_2 was decreased to 50 ppm, increased to 400 ppm, and finally increased to 1,250 ppm. Data was logged after 90 to 120 s at each CO_2 concentration. Table: Maximum Rubisco activity ($V_{c,max}$) and maximum electron transport rate used in RuBP regeneration (J_{max}). C, F) pmf; D, G) proton conductance of ATP synthase (gH^+); *E*, H) proton flux (vH^+). (C)– (E) Measurements were taken during photosynthetic induction at the indicated time points using 169 µmol photons

(continued)

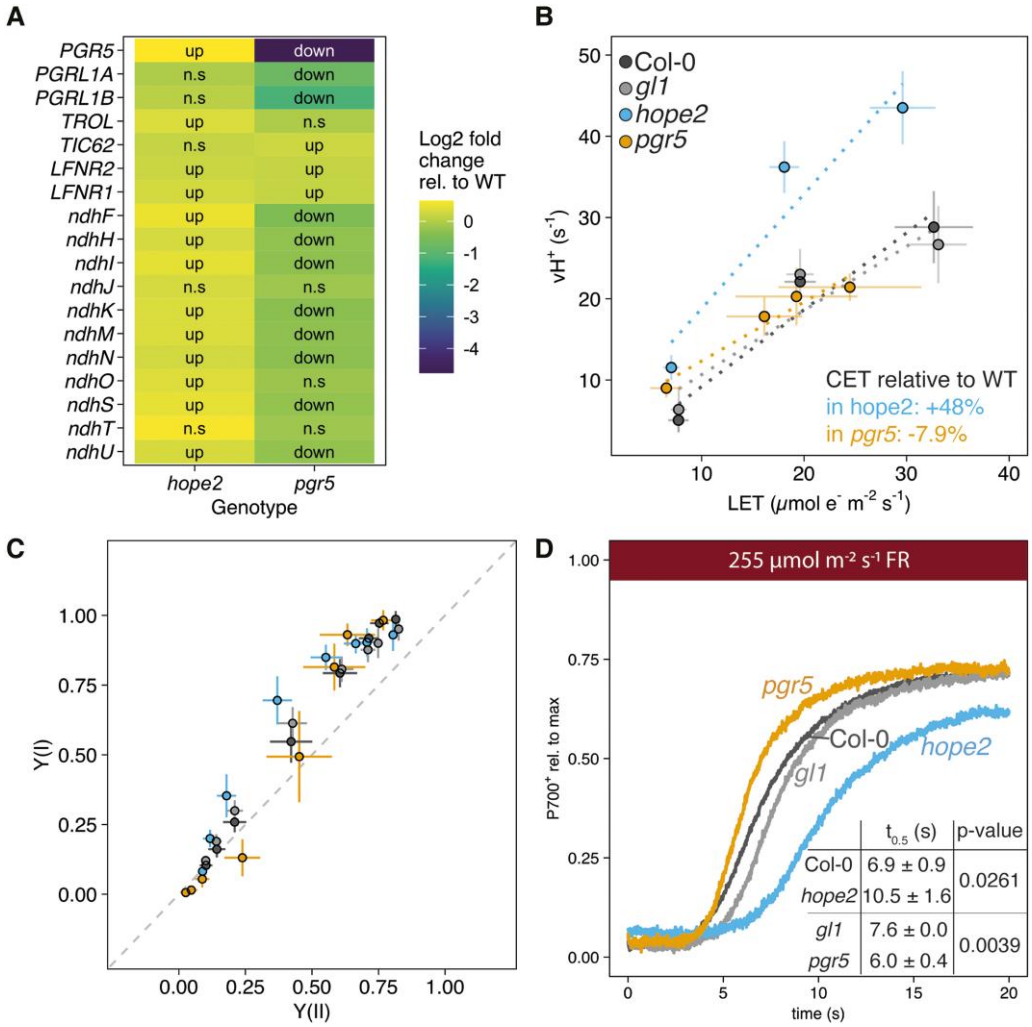

Figure 2. Measurements of cyclic electron transfer. A) Abundance of proteins involved in CET, normalized to wild type. B) Proton flux versus LET. Higher flux at similar LET indicates increased cyclic electron transfer. C) Yield of photosystem I versus yield of photosystem II. D) P700 oxidation during FR light. Prior to FR light, leaves were exposed to a weak ML for 30 s, followed by a SP and 30 s of darkness. Data was normalized to maximal P700 oxidation after 30 s FR light and a SP. Insert: Half-life of P700 oxidation determined by fitting an allosteric sigmoidal function prior to the SP. Data points represent the average of three to six biological replicates ± SD. Different letters indicate statistical significance between genotypes at each time point, calculated from a Tukey HSD test, alpha = 0.05. In (A) "Up" refers to significantly ($P < 0.05$) more abundant proteins and "down" significantly ($P > 0.05$) less abundant proteins, "n.s." = not significant.

increase) showed significantly increased abundance in *hope2* (Fig. 2A). Interestingly, however, PGRL1 was unchanged in *hope2* (Fig. 2A). Increased abundance in *hope2* was also seen for LFNR1 and LFNR2 and their membrane tether, thylakoid rhodanese-like protein, which have been recently linked to CET (Kramer et al. 2021). On the other hand, in *pgr5*, both PGRL1 isoforms and NDH subunits were decreased by ~0.70- to 1.31-fold and ~0.21- to 0.35-fold, respectively (Fig. 2A), as shown previously by immunoblotting (Munekage et al. 2004; Nikkanen et al. 2018; Wada et al. 2021). Given these results we hypothesized that pmf may be maintained in *hope2* via increased CET relative to wild type. A well-established method of assessing changes in CET is the relationship between vH^+ and LET (calculated by chlorophyll fluorescence)

Figure 1. (Continued)
m^{-s} s^{-1} actinic light. (F)–(H) Measurements were taken after 5 min at each indicated light intensity. Data points represent the average of three to seven biological replicates ± SD. Different letters indicate statistical significance between genotypes at each time point, light intensity or C_i, calculated from a Tukey HSD test, alpha = 0.05. Bold *P*-values in (B) indicate significantly different $V_{c,\ max}$ and J_{max} between Col-0 and *hope2*, calculated from a two-sided *t*-test, alpha = 0.05.

(Okegawa et al. 2005; Livingston et al. 2010a, b; Strand et al. 2015, 2017). A steeper slope indicates a greater contribution of CET to vH^+. In *hope2*, the relationship between vH^+ and LET was significantly ($P < 0.05$) steeper than in the wild-type Col-0, with a slightly shallower slope observed in *pgr5* (Fig. 2B). We estimate from the slope that vH^+ is decreased by 7.9% in *pgr5*, similar to the 13% previously determined by this method (Avenson et al. 2005), but increased by 48% in *hope2*. Deviation of a linear relationship between the quantum yields of PSI (Y(I)) and PSII (Y(II)) at varying light intensities provides another indication of CET capacity (Okegawa et al. 2005; Livingston et al. 2010a, b; Strand et al. 2015, 2017). Consistent with higher CET in *hope2* we found increased Y(I) relative to Y(II) compared to the wild type, while the smallest deviation was found in *pgr5* (Fig. 2C). An alternative complementary method of assessing CET in vivo involves following the rate of P700 oxidation induced by far red (FR) light which preferentially excites PSI (Joliot and Joliot 2002; Okegawa et al. 2007; Rühle et al. 2021). In this assay, decreased CET activity results in faster P700 oxidation and lower half-times ($t_{0.5}$), whereas increased CET has the opposite effect (Joliot and Joliot 2002; Joliot and Johnson 2011; Rühle et al. 2021). Consistent with lower CET in *pgr5*, FR light-induced P700 oxidation was faster than wild-type *gl1* (Fig. 2D). However, P700 oxidation $t_{0.5}$ in *hope2* was significantly ($P = 0.0200$) slower than Col-0 (Fig. 2D), in line with increased CET relative to wild-type Col-0. We confirmed that these differences in P700 oxidation rate could not be ascribed to differences in antenna size between the wild-type Col-0 and *hope2* by infiltration of leaves with DCMU and methyl viologen, which eliminate donor and acceptor side limitations on PSI (Supplemental Fig. S2).

PGR5 is the major CET pathway in *hope2*

Since both NDH and PGR5 abundance increased in *hope2* we sought to ascertain whether one or both pathways contributed to the observed increases in CET and vH^+. To that end the double mutants *hope2 ndho* and *hope2 pgr5* were created and verified by DNA sequencing for the *hope2* mutation and immunoblotting for NdhS, PGR5, and PGRL1 levels (Supplemental Fig. S3). Previous high CET mutants have involved the NDH pathway (Livingston et al. 2010a, b; Strand et al. 2015, 2017), which prompted us to first analyze the *hope2 ndho* double mutant. At light levels above 250 µmol photons m^{-2} s^{-1}, pmf in the *hope2 ndho* double mutant was not significantly different to the *hope2* and *ndho* single mutants (Fig. 3A), though both *ndho* and *hope2 ndho* showed slightly lower pmf than the wild type, consistent with past results (Nikkanen et al. 2018). Similarly, gH^+ and vH^+ were largely unchanged in *hope2 ndho* compared to *hope2*, which were both significantly higher than *ndho* and wild type (Fig. 3, B and C). The NPQ level in the *hope2* mutant was wild type-like, whereas *ndho* showed higher NPQ as previously reported (Rumeau et al. 2005; Takagi et al. 2017). The *hope2 ndho* mutant showed an NPQ level between *hope2* and *ndho*, demonstrating that NPQ in *hope2* does not require NDH (Fig. 3D), although clearly elevated NPQ in *ndho* is affected by loss of gH^+ regulation. The PSII quantum yield (Y(II)) and PSII Q_A^- reduction (1-qL) were similar in *hope2 ndho* and *hope2*, only low light had a moderate effect (Fig. 3, E and F). The PSI quantum yield (Y(I)) is increased in *hope2* relative to the wild type at moderate light intensities between 250 and 500 µmol photons m^{-2} s^{-1}, whereas *hope2 ndho* and *ndho* were lower than wild type and *hope2* at low light but was similar at higher light intensities (Fig. 3G). Finally, PSI donor-side limitation (Y(ND)) and PSI acceptor-side limitation (Y(NA)) in *hope2 ndho* were also similar to *hope2*, which were significantly lower than the wild type and *ndho* (Fig. 3, H and I). CET measured via the relationship between vH^+ and LET or Y(I) and Y(II) in *ndho* was similar to wild type, whereas *hope2 ndho* behaved largely like *hope2*, with only slight deviation seen at the lowest LET levels (Fig. 3, J and K), suggesting the major contribution of the NDH pathway is in low light. Furthermore, CET measured via the P700 oxidation method in *hope2 ndho* showed it was unchanged compared to *hope2* ($P = 0.2424$), suggesting the elevated CET is little affected by the absence of the NDH pathway under FR illumination (Fig. 3L).

Since removal of NDH from the *hope2* background did not strongly affect the enhanced vH^+ in *hope2*, we next examined the effect of loss of PGR5. The Arabidopsis *pgr5* mutant has recently been shown to have point mutations in two separate genes encoding the PGR5 and PPT1 proteins, the latter of which seems to perpetuate long-term damage to PSI (Wada et al. 2021). Importantly for the conclusions of this work, however, the low pmf and Y(ND) phenotypes were shown to be associated with the PGR5 mutation alone, consistent with tDNA knock-out results in rice and a recent CRISPR-Cas9 *pgr5* mutant generated in *Arabidopsis* (Nishikawa et al. 2012; Penzler et al. 2022). Pmf and vH^+ in the *hope2 pgr5* double mutant dropped significantly below *hope2*, except under very low light (Fig. 4, A and C), whereas gH^+ was similar in *hope2* and *hope2 pgr5* (Fig. 4B). In line with this, NPQ and Y(II) were lower in *hope2 pgr5* and 1-qL was higher compared to *hope2* (Fig. 4, D–F). Y(I) was also substantially lower at all light levels in *hope2 pgr5* compared to *hope2* (Fig. 4G). Y(ND) remained low in the *hope2 pgr5* double mutant, similar to the respective single mutants (Fig. 4H) and Y(NA) in *hope2 pgr5* was similar to *pgr5* and elevated with respect to *hope2* (Fig. 4I). CET measured via the relationship between vH^+ and LET or Y(I) and Y(II) was significantly less steep ($P = 0.008$) in *hope2 pgr5* compared to *hope2* and resembled wild type (Fig. 4, J and K). In line with this, FR-induced P700 oxidation in *hope2 pgr5* was also much faster than in *hope2*, indicating that the increased CET is abolished and consistent with this the $t_{0.5}$ was significantly lower than *hope2* ($P < 0.0001$) (Fig. 4L). Overall, these data show that in *hope2*, PGR5-dependent CET is required to maintain wild-type level of pmf by increasing vH^+, whereas NDH-dependent CET only makes a substantial contribution to pmf in the *hope2* background at lower light intensities. We verified this furthermore by growing genotypes under

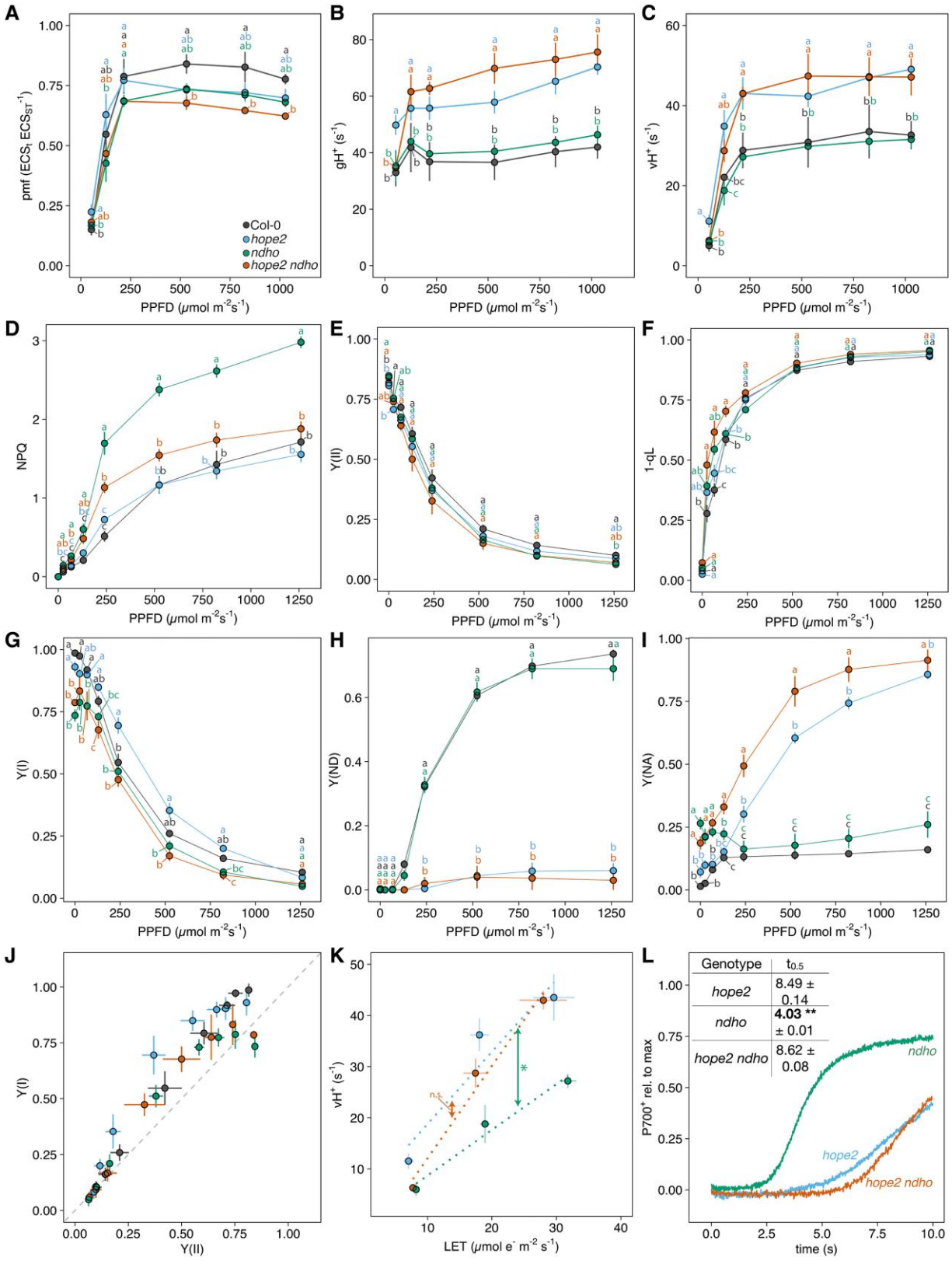

Figure 3. Photosynthetic parameters and CET measurements in *hope2 ndho*. A) pmf. B) Proton conductance of ATP synthase (gH$^+$). C) Proton flux (vH$^+$). D) NPQ. E) Quantum yield of photosystem II (Y(II)). F) 1-qL (PSII acceptor-side limitation). G) Quantum yield of photosystem I (Y(I)), H) Donor-side limitation of PSI (Y(ND)). I) Acceptor-side limitation of PSI (Y(NA)). J) Y(I) versus Y(II). K) Proton flux versus linear electron transfer. L) P700 oxidation during FR light, insert: $t_{0.5}$ (s). Data points represent the average of three to six biological replicates ± SD. Different letters indicate statistical significance between genotypes at each light intensity, calculated from a Tukey HSD test, alpha = 0.05. Asterisks in (K) and (L) indicate $P <$ 0.001 calculated from a one-way ANOVA of slopes or $t_{0.5}$ between either *hope2* and *ndho* or *hope2 ndho*. n.s. indicates "not significant".

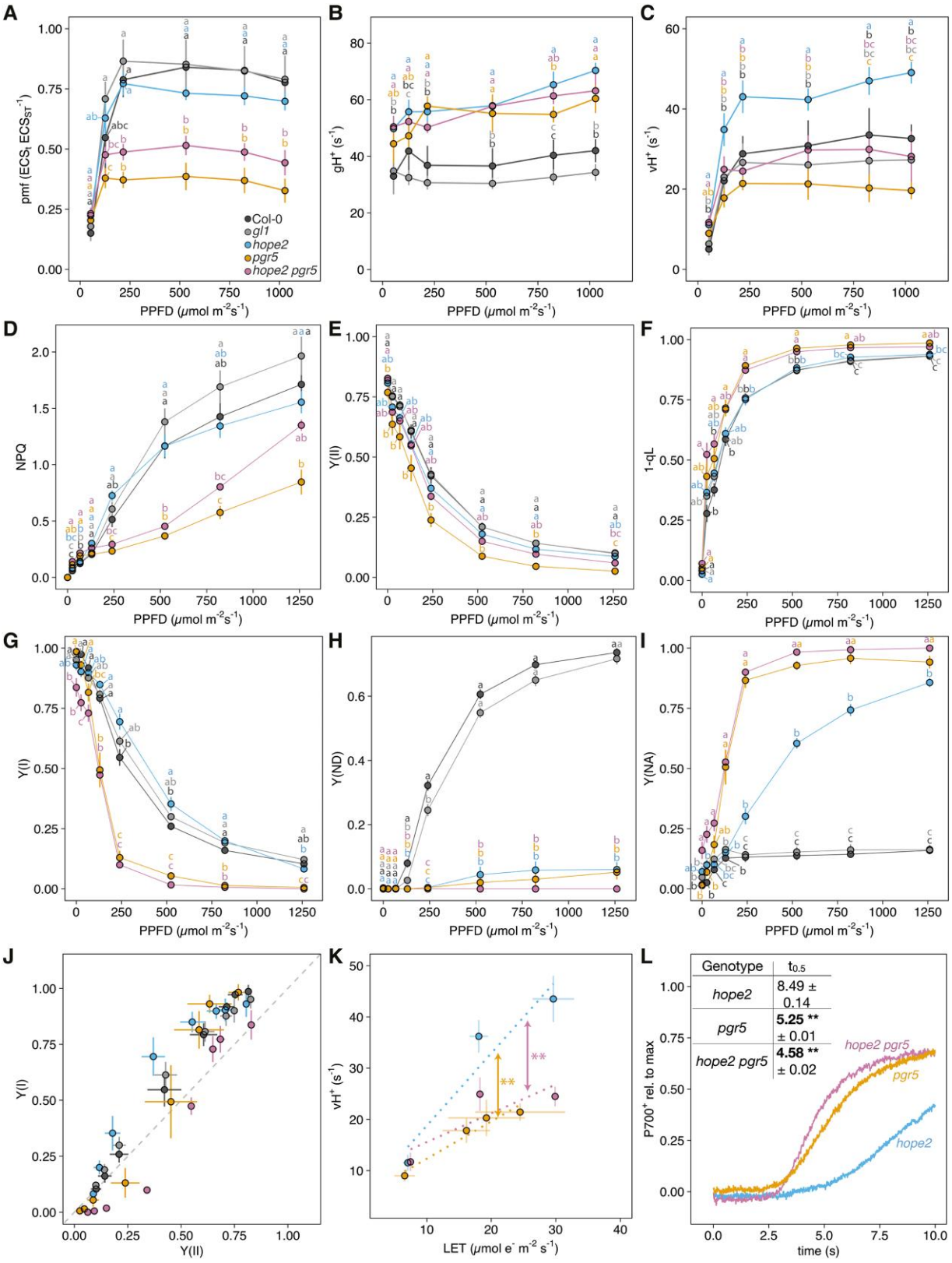

Figure 4. Photosynthetic parameters and CET measurements in *hope2 pgr5*. A) pmf. B) Proton conductance of ATP synthase (gH$^+$). C) Proton flux (vH$^+$). D) NPQ. E) Quantum yield of photosystem II (Y(II)). F) 1-qL (PSII acceptor-side limitation). G) Quantum yield of photosystem I (Y(I)); H) Donor-side limitation of PSI (Y(ND)). I) Acceptor-side limitation of PSI (Y(NA)). J) Y(I) versus Y(II). K) Proton flux versus linear electron transfer. L) P700 oxidation during FR light, insert: $t_{0.5}$ (s). Data points represent the average of three to six biological replicates ± SD. Different letters indicate statistical significance between genotypes at each light intensity, calculated from a Tukey HSD test, alpha = 0.05. Asterisks in (K) and (L) indicate $P <$ 0.001 calculated from a one-way ANOVA of slopes or $t_{0.5}$ between either *hope2* and *pgr5* or *hope2 pgr5*.

control and high light conditions. This showed that plant rosette area and fresh weight were significantly impaired in *hope2 pgr5* but to a lesser extent in *hope2 ndho* (Supplemental Fig. S4). Furthermore, F_v/F_m in *pgr5* and *hope2 pgr5* was significantly impaired after high light treatment.

Photosynthetic control is absent in *hope2* despite maintenance of wild-type levels of ΔpH

The maintenance of wild-type levels of pmf in *hope2* due to increased PGR5-dependent CET raised the question of why NPQ is wild type-like, while Y(ND) is *pgr5*-like? One possibility is that the pmf is differently partitioned between the ΔpH and $\Delta\Psi$ components in *hope2*, which given the differing reported sensitivity of NPQ and Y(ND) to ΔpH might explain their contrasting responses (Horton et al. 1991; Nishio and Whitmarsh 1993). Indeed, our proteomic data shows an increase in the relative abundance of the putative H^+/K^+ thylakoid antiporter KEA3, which could modify the ΔpH/$\Delta\Psi$ partitioning of pmf in this mutant (Supplemental Fig. S1). To test these ideas further we first confirmed that NPQ in *hope2* was of the ΔpH-dependent rapidly-relaxing qE type rather than photoinhibitory or sustained qI-type quenching (Supplemental Fig. S5). Next, we utilized the ECS partition method to assess the relative ΔpH and $\Delta\Psi$ contributions to pmf. Previous ECS partitioning data suggested *hope2* may have a slightly lower ΔpH contribution to pmf (Takagi et al. 2017). However, this method has recently been called into question due to the overlapping absorption changes associated with qE which lead to overestimation of $\Delta\Psi$ contributions to pmf, particularly when zeaxanthin synthesis is incomplete (Wilson *et al.* 2021). We thus compared using the partition method the pmf composition under conditions where zeaxanthin synthesis was incomplete (increasing light intensity every 20 s) versus complete (decreasing light intensity following 10 min illumination at 1,421 µmol photons m^{-2} s^{-1}). The results showed that pmf takes longer to establish in *hope2* consistent with the data in Fig. 1C, as a result the apparent $\Delta\Psi$ contribution to pmf is larger in *hope2* than in the wild type (Fig. 5, A and B). By contrast, once pmf is established after 10 min of high light little difference in either the extent of pmf or the relative $\Delta\Psi$ versus ΔpH contribution was observed between *hope2* and the wild type (Fig. 5, B, C). In line with this, while NPQ is smaller in *hope2* during induction compared to the wild type, once pmf is fully established in *hope2* NPQ reaches WT levels (Fig. 5D). Yet, in spite of this Y(ND) remains much smaller and Y(NA) much larger in *hope2* (Fig. 5, E and F). Therefore, lower Y(ND) in *hope2* cannot be ascribed to lower ΔpH contribution to pmf.

Discussion

Hope2 is able to maintain CO_2 assimilation through increased CET

Proton motive force is harnessed for the production of ATP by ATP synthase, while its major ΔpH component also plays an important regulatory role triggering qE and Y(ND). *Hope2*, a recently described G134D γ1-subunit mutant in Arabidopsis was particularly interesting because it showed a similar phenotype compared to *pgr5* with respect to the loss of photosynthetic control and high gH^+ but key differences with respect to qE and CO_2 assimilation (Munekage et al. 2004; Takagi et al. 2017). Thus, ATP-synthase regulation and CET may play distinct roles in the regulation of photoprotection and ATP/NADPH balance. Here we show that despite high gH^+, *hope2* is able to maintain pmf at wild-type levels through increased vH^+. The normal pmf levels we observe in *hope2* are a key point of difference with the previous study by Takagi et al. (2017). In this previous study, pmf was more variable, being lower than wild type under low O_2 or ambient CO_2 without preillumination and similar following preillumination. We found these differences could be explained by the slower establishment of pmf in *hope2* (Figs. 1, C, D, and 5A). Comparison of the respective quantum yields of PSI and PSII showed increased electron transfer rate through PSI in *hope2* compared to wild type consistent with enhanced CET (summarized in Fig. 6). CET is notoriously difficult to measure owing to the fact that it produces no net product and utilizes a common set of spectroscopically active-redox carriers with LET. Nonetheless, careful comparison of vH^+ with the rate of LET demonstrates a steeper relationship in *hope2*, consistent with the phenotype seen in other high CET mutants previously described (Livingston et al. 2010a, b; Strand et al. 2015, 2017). A complementary method for assessing CET involves illumination monitoring the rate of P700 oxidation with FR. Consistent with the vH^+/LET method the FR oxidation of PSI is slower in *hope2* confirming an increased rate of CET. The slower establishment of pmf in *hope2* (Fig. 1, C and D) seems to reflect the varying timescales for relaxation of ATP synthase and activation of CET. Thus, in the first few moments following illumination increases in pmf depend largely on the restricted gH^+ in the wild type. As the ATP-synthase regulatory γ1-subunit thiol becomes gradually reduced in the light gH^+ increases (Konno et al. 2012). Following this increase in gH^+, vH^+ must be increased if pmf is to be maintained. The maintenance of wild-type-levels of pmf likely explains the similar CO_2 assimilation rates in *hope2* compared to the wild type and is further evidence for an important role of CET in ensuring the optimal ATP/NADPH ratio.

Enhanced CET in *hope2* depends on the PGR5-dependent rather than NDH-dependent pathway

A proteomic comparison of the thylakoid membranes from *hope2* and wild-type plants showed that NDH and PGR5 abundance was upregulated. We therefore constructed the double mutants *hope2 pgr5* and *hope2 ndho*, to understand the respective contributions of the two pathways to increased CET in *hope2*. The steeper vH^+ versus LET and Y(I) versus (YII) slopes and slower FR-driven P700 oxidation

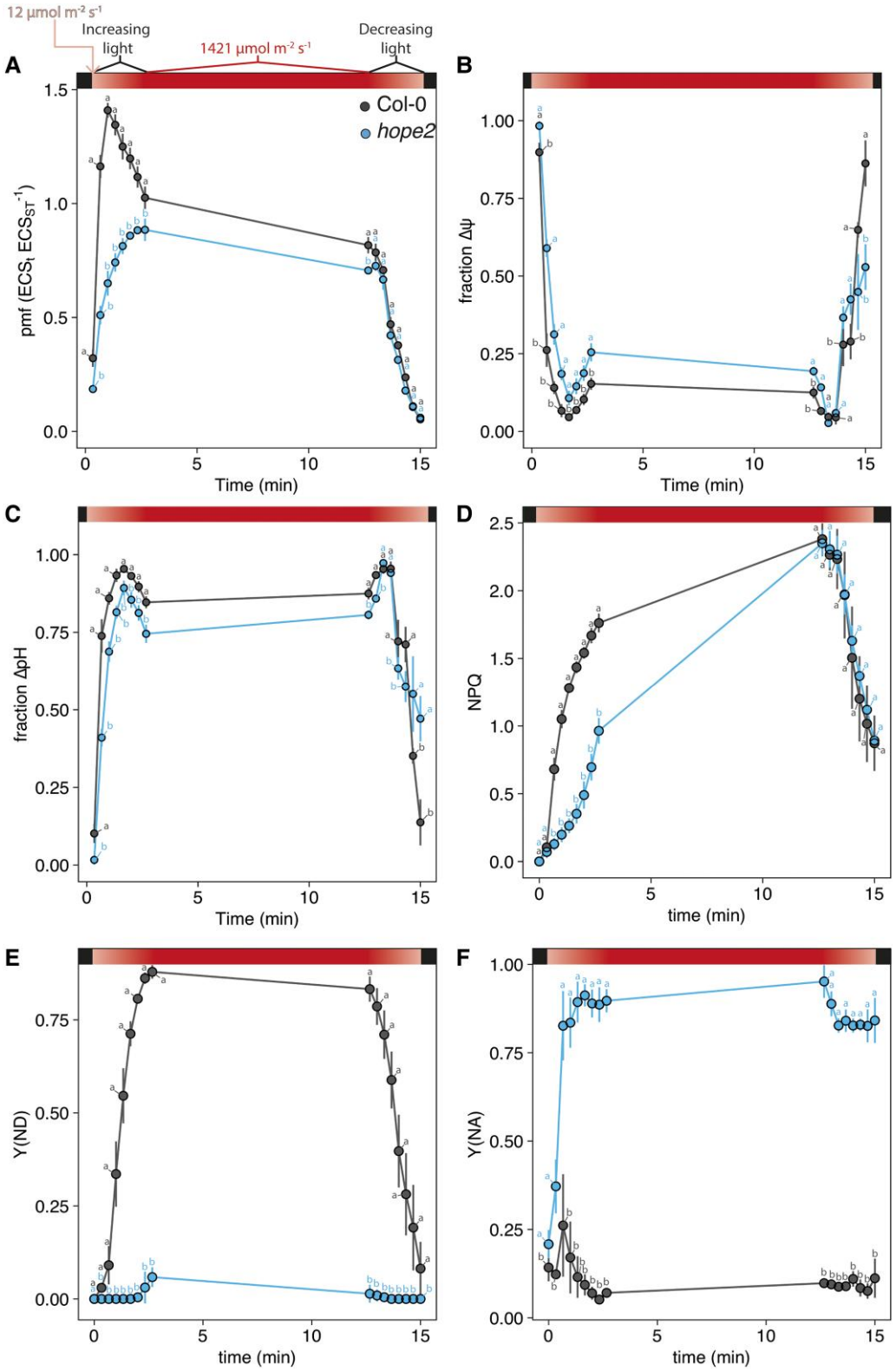

Figure 5. Response of Col-0 and *hope2* to rapidly increasing and decreasing light intensities. A) pmf. B) Fraction of $\Delta\psi$ contribution. C) Fraction of ΔpH contribution. D) NPQ. E) Donor-side limitation of PSI (Y(ND)). F) Acceptor-side limitation of PSI (Y(NA)). Rapid changes from low (12 µmol photons m^{-2} s^{-1}) to high (1,421 µmol photons m^{-2} s^{-1}) light are indicated at the top of panel a by a red color gradient. Light levels were increased every 20 s, kept at high light for 10 min and decreased every 20 s. Data points represent the average of three biological replicates ± SD. Different letters indicate statistical significance between genotypes at each light intensity, calculated from a Tukey HSD test, alpha = 0.05.

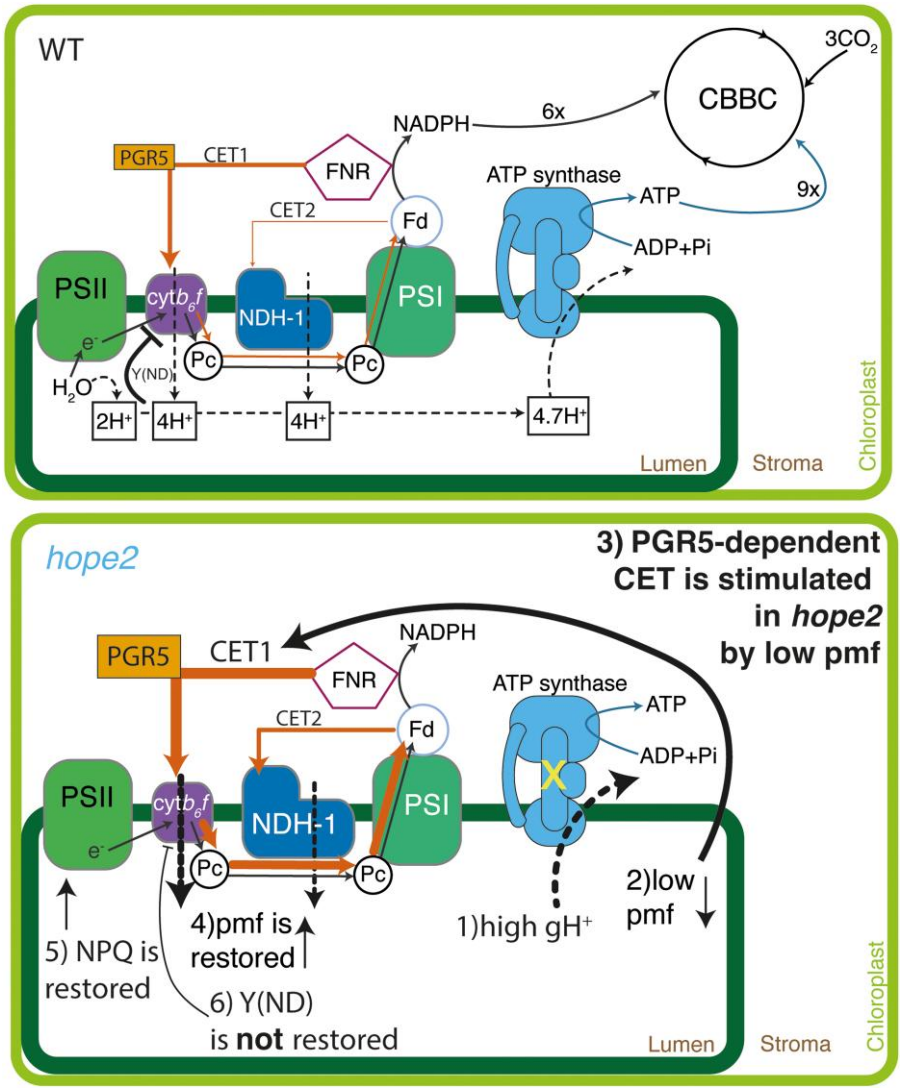

Figure 6. Proposed model of PGR5-dependent supercharged CET in *hope2*. In wild-type, CET is dominated by PGR5 to produce extra pmf and ATP. CET2 via NDH is more important at low light. Regulation of ATP synthase in *hope2* is disturbed, resulting in high gH^+ and low pmf. In response, PGR5 levels are increased, and to a lesser extent, NDH levels, too. This increases CET1 and restores pmf and NPQ. However, Y(ND) is not restored, suggesting that regulation of ATP synthase is crucial for PSI photoprotection. PSII, Photosystem II; cytb_6f, cytochrome b_6f complex; NDH-1, NAD(P)H:plastoquinone dehydrogenase complex 1; PSI, Photosystem I; FNR, ferredoxin:NADP(H) oxidoreductase; CBBC, Calvin–Benson–Bassham Cycle; Y(ND), donor-side regulation.

seen in *hope2* were lost in *hope2 pgr5* double mutant, and it suffered from the more extreme PSI acceptor side limitation (Y(NA)) seen in *pgr5*. By contrast, the phenotype of the *hope2 ndho* double mutant was less dramatic, with a similar rate of P700 oxidation to *hope2*, with only a slight decrease in the vH^+/LET slope seen at low light and although there was an increase in Y(NA) compared to *hope2* this was less severe than in *hope2 pgr5*. The predominant reliance of *hope2* on the PGR5-dependent CET1 pathway is key point of difference compared to other previously characterized high cyclic electron flow (*hcef*) mutants, which use the NDH-dependent CET2 pathway (Livingston et al. 2010a, b). The factors regulating CET1 and CET2 have yet to be fully elucidated (Yamori and Shikanai 2015; Yamori et al. 2016), though H_2O_2 signaling and $NADPH/NADP^+$ redox balance have been recently implicated in control of the NDH and PGR5 pathways, respectively (Strand et al. 2015, 2016). However, since Y(NA) is high in *hope2*, both signals would be expected, consistent with the increased abundance of both PGR5 (0.56-fold increase) and NDH subunits (0.21- to 0.41-fold increase) we find in this mutant. By contrast, quantification of NDH levels by immunoblotting in *hcef1* revealed a 15-fold increase in NDH and a 50% decrease in PGR5 (Livingston et al. 2010a). Comparison of *hope2* and *hcef1* reveals a large difference in gH^+ between the mutants. Therefore, if pmf can be restored by combination of ATP synthase gH^+ downregulation and increases in NDH-dependent CET2, it may negate the need for upregulation of PGR5. It may be important in

this regard that we see the greatest contribution of the NDH-pathway (H^+/e^- ratio of 4) in *hope2* under low light, where it is less thermodynamically limited by backpressure from the pmf (Strand et al. 2017). This is in line with previous work showing *ndho* and *crr* mutants show more substantial phenotypes in low light situations (Yamori et al. 2011, 2015; Wang et al. 2015; Yamori and Shikanai 2015). By contrast, the lower efficiency PGR5 pathway (H^+/e^- ratio of 2) may be preferred in high light, consistent with the stronger phenotype of *pgr5* plants under such conditions (Munekage et al. 2004). Therefore, a combination of simple competition for excess electrons at the PSI acceptor side and thermodynamic constraints on turnover may determine which CET pathway is favored in particular circumstances. Irrespective, the isolation of a high CET mutant that depends on PGR5 is important since the steady-state contribution of CET1 is generally estimated to be low (<13% of LET) and difficult to measure. *Hope2* is therefore a useful tool for future research on PGR5-dependent CET1.

High CET in the absence of ATP-synthase regulation fails to restore photosynthetic control

Previously, repetitive flash treatment showed that PSI in *hope2* was, similar to *pgr5*, susceptible to photoinhibition (Takagi et al. 2017). However, it was unclear whether the *pgr5* phenotype was primarily due to loss of gH^+ control or loss of CET1 (Avenson et al. 2005; Yamamoto and Shikanai 2020). While the maintenance of wild-type-levels of pmf through enhanced CET in *hope2* allowed normal qE-levels to develop, Y(ND) remained virtually absent (summarized in Fig. 6). *Prima facie*, this suggests that gH^+ regulation of ATP synthase is crucial for photosynthetic control. Accordingly, even strongly enhanced PGR5-dependent CET1 does not protect against PSI photoinhibition in *hope2*. The failure of CET to protect PSI is consistent with recent results showing that both CET1 and CET2 do not act as photoprotective electron sinks in the absence of other mechanisms of acceptor side regulation of PSI (Rantala et al. 2020). Since photosynthetic control relies on the low lumenal pH-induced slowdown of PQH_2 oxidation by the Rieske iron–sulfur protein of cytb_6f (Nishio and Whitmarsh 1993; Jahns et al. 2002), the most logical explanation for loss of Y(ND) is a loss of ΔpH in *hope2*. Previously, a difference in relative partitioning of pmf into $\Delta\Psi$ and ΔpH compared to the − was found in *hope2* (Takagi et al. 2017). However, we traced these apparent differences in partitioning to a slower establishment of pmf in *hope2*, which leads to increased overlap with the qE-related absorption changes as described for the *npq1* mutant lacking zeaxanthin (Wilson et al. 2021). Once pmf is established in *hope2*, and presumably zeaxanthin synthesis is completed, then no major differences in the amplitude of ΔpH between *hope2* and the wild type are present. Therefore, changes in ΔpH are not the cause of the low photosynthetic control phenotype in *hope2*. These data mirror similar reports in *pgr5* plants overexpressing the *Chlamydomonas reinhardtii* plastid terminal oxidase 2 protein and the FNR antisense mutant of *N. benthamiana*, both of which showed normal qE but lacked photosynthetic control (Hald et al. 2008; Zhou et al. 2022). One possibility is that just the relationship between qE and ΔpH is modified by the xanthophyll cycle de-epoxidation state (Rees et al. 1989; Horton et al. 1991), so the relationship between Y(ND) and ΔpH is regulated by NADPH/$NADP^+$ redox poise (Johnson 2003; Hald et al. 2008). In *hope2* where Y(NA) is high, NADPH/$NADP^+$ redox poise is likely disturbed. The fact that Y(ND) can be restored in *pgr5* in the presence of the artificial PSI electron acceptor methyl viologen (Munekage et al. 2002; Wang et al. 2018) or via transgenic expression of *Physcomitrium patens* Flv proteins (Yamamoto et al. 2016) could be interpreted as further evidence for this hypothesis. Further work is now required to test these ideas.

The nature of the mis-regulation of ATP synthase in *hope2*

The nature of the mis-regulation of ATP synthase in *hope2* remains unclear. Previously Takagi et al. (2017) showed that gH^+ in *hope2* fails to respond to CO_2 concentration suggesting either metabolic control may be lost in this mutant or that the mutant enzyme is less efficient than the wild-type version. The mechanism of metabolic control of the ATP synthase is still unclear, though gH^+ is known to be sensitive to Pi, NADPH/$NADP^+$ redox poise in addition to CO_2 concentration suggesting it is able to sense the stromal metabolism and so tune ATP production accordingly (Velthuys 1978; Kanazawa and Kramer 2002; Avenson et al. 2005; Takizawa et al. 2008; Kohzuma et al. 2013). The G134D mutation in the γ1-subunit of *hope2* ATP synthase is in the GxxGxxG NADP(H)-binding motif of the Rossman fold domain. This motif of the γ1-subunit is conserved in ATP synthases from chloroplasts and cyanobacteria (GxxGxxG), mitochondria (TxxGxxG), and *Escherichia coli* (SxxGxxG) (Supplemental Fig. S6) although its function remains unknown. Given the previous demonstration that NADPH/$NADP^+$ redox poise can affect the gH^+ of the ATP synthase in *Chlamydomonas* (Velthuys 1978), one possibility is that the Rossman fold is the site of metabolic regulation of the ATP-synthase complex. However, several of our observations are more closely aligned with the leak hypothesis. Firstly, we observe that gH^+ starts at a higher value during the dark to light transition in *hope2* suggesting the mutant enzyme is affected in both its oxidized and reduced states (Fig. 1D). Secondly, if high gH^+ in *hope2* were producing a higher ATP/ADP ratio in *hope2* compared to the wild type one would expect that it would increase the capacity for CO_2 assimilation under high CO_2 conditions, something which we do not observe (Fig. 1B). Rather our data suggest that *hope2* is having to "peddle faster" to obtain the wild-type ATP/ADP ratio via increasing CET, as discussed above. Indeed, the C87K mutation in the Rossman fold motif of the *E. coli* ATP synthase γ-subunit (C139 in Arabidopsis) has been shown to decrease the

coupling efficiency between the Fo rotor and F1 head, increasing the effective H^+/ATP ratio (Li et al. 2019). Therefore, the G134D mutation in close proximity to this region of the protein could produce a similar effect in Arabidopsis.

Conclusions

Our data have clarified the respective importance of proton influx and efflux control in photosynthetic regulation. We found ATP synthase gH^+ regulation is indispensable for photosynthetic control, even when CET can maintain pmf to ensure an optimal ATP/NADPH ratio and qE. This work highlights the interconnectedness and mutual dependence of the various photoprotective regulatory mechanisms in addition to the remarkable ability of the photosynthetic apparatus to preserve pmf via molecular plasticity in thylakoid protein composition.

Materials and methods

Plant material, growth conditions, generation of double crosses and growth experiment

Arabidopsis thaliana mutants *hope2* and the wild-type background Col-0 and *pgr5* and the wild-type background *gl1* were grown in a controlled-environment chamber for at least 6 wk at 21 °C /15 °C day/night, 60% relative humidity with an 8-h photoperiod at a light intensity of 200 µmol photons m^{-2} s^{-1}. Double mutants were generated by crossing *hope2* with either *pgr5* or *ndho*. Seeds from successful crosses were sown and allowed to self-fertilize. Seedlings were screened for the *pgr5* phenotype using an Imaging PAM (Heinz Walz GmbH, Effeltrich, Germany). Plants with low NPQ were then screened for the high gH^+ phenotype, characteristic for *hope2*, using the Dual PAM (Heinz Walz GmbH, Effeltrich, Germany). Crosses displaying both phenotypes were used for thylakoid isolation (described below). Western blots were performed on isolated thylakoids using the NdhS (AS164066, 1:5,000 dilution) and PGR5 (AS163985, 1:1,300 dilution) antibodies (all purchased from Agrisera, Vännäs, Sweden). Homozygosity for *hope2* was verified by Sanger sequencing, using the primers 5′-ACT TCCTCACCTCCTTCACG-3′ and 5′-AATTTCCCTTCTTGC CCACG-3′. For the growth experiment, 12 biological replicates of each genotype were randomly distributed in a 4 × 6 seed tray for control and high light treatment. After 3 wk in control conditions, the first rosette area measurement was taken. Half of the trays were then transferred to medium light (400 µmol photons m^{-2} s^{-1}) for 1 wk. Plants were then shifted to high light (685 µmol photons m^{-2} s^{-1}) for 18 d. At the end of the growth experiment (day 24), a subset of plants of each genotype and growth light was used for F_v/F_m determination and fresh weight of all plants was determined as well. Rosette areas were measured using the iDIEL Plant Software (Dobrescu et al. 2017).

Chlorophyll fluorescence and in situ P700 absorption spectroscopy

A Dual-KLAS-NIR photosynthesis analyzer (Heinz Walz GmbH, Effeltrich, Germany) was used for pulse-amplitude modulation chlorophyll fluorescence measurements and P700 absorption spectroscopy in the near-infrared (Klughammer and Schreiber 2016; Schreiber and Klughammer 2016). After plants had dark-adapted for at least 1 h, four pairs of pulse-modulated NIR measuring beans were zeroed and calibrated before each measurement. For each genotype, one leaf was used to generate differential model plots according to manufacturer's protocol, which were used for online deconvolution to determine redox changes of P700. Prior to each measurement, maximum oxidation of P700 was determined by using the preprogrammed NIRmax routine. This consisted of a 3 s pulse of 635 nm actinic light on top of which a 30 ms multiple turnover flash (MT) was given after 800 ms, followed by 4 s of darkness and 10 s of 255 µmol photons m^{-2} s^{-1} 740 nm FR light and a MT at the end to achieve full oxidation of P700. NIRmax values were determined by using the preprogrammed "Get Max-Values" option. Dark-fluorescence (F_0) and maximal fluorescence (F_m) were determined prior to light or induction curves. Photosynthetic parameters were determined by using measuring beam intensities of 20 µmol photons m^{-2} s^{-1} and 14 µmol photons m^{-2} s^{-1} for chlorophyll fluorescence and P700 redox changes, respectively and a 18,000 µmol photons m^{-2} s^{-1} saturating pulse. Photosynthetic parameters were calculated as follows: $Y(II) = (F'_m - F)/F'_m$, $NPQ = (F_m - F'_m)/F'_m$, $Y(I) = (P'_m - P)/P_m$, $Y(NA) = (P_m - P'_m)/P_m$, $Y(ND) = (P - P_0)/P_m$. For light curves, measurements were taken after 5 min at each light intensity. For induction curves, AL intensity was set to 169 µmol photons m^{-2} s^{-1} and measurements were taken at multiple time points after AL was turned on. To determine P700 oxidation for CET determination, leaves were exposed to a weak measuring light for 30 s, followed by a MT. FR light was then turned on for 20 s. Half-time of P700 oxidation was determined by fitting an allosteric sigmoidal function (Graphpad Prism, 9.1.1).

Electrochromic shift measurements

Electrochromic shift was measured using a Dual-PAM analyzer with a P515/535 emitter/detector module (Heinz Walz GmbH, Effeltrich, Germany) (Klughammer et al. 2013). Plants were dark-adapted for at least 1 h prior to measurements. Proton motive force was calculated from the decay of the P515 signal when 635 nm AL was turned off, by fitting a single exponential decay to the first 300 ms in the dark to determine the span of the signal decay (ECS_t). pmf was normalized by dividing ECS_t by the magnitude of a 50 µs ST flash applied prior to account for leaf thickness and chloroplast density (Takizawa et al. 2007; Livingston et al. 2010a; Wang et al. 2015; Takagi et al. 2017). The proton conductance gH^+ was calculated as the inverse of the decay time constant

τ_{ECS} of the single exponential decay and proton flux was calculated as $vH^+ = pmf \times gH^+$ (Baker et al. 2007).

Leaf infiltration

Dark-adapted leaves were vacuum-infiltrated with 30 µM DCMU and 100 µM methyl viologen buffered in 20 mM HEPES (pH 7.5), 150 mM sorbitol, and 50 mM NaCl. Leaves were dark-adapted for 10 min between infiltration and measurements.

Gas exchange

CO_2-response (AC_i) and light-response curves (AQ) were measured using the infrared gas analyzer system 6400-XT (LiCOR Biosciences, Lincoln, NE, USA). Prior to measurements, plants were exposed to 400 ppm reference CO_2, 1,500 µmol photons m^{-2} s^{-2} light at 25 °C and approximately 50% relative humidity for at least 10 min until steady-state was reached and stomata were wide open with a C_i/C_a of >0.7. For AC_i curves, data was logged at various CO_2 concentrations after 90 to 120 s using the following sequence of reference CO_2 concentrations, as recommended by (Busch 2018): 400, 350, 300, 250, 200, 150, 100, 50, 400, 400, 450, 500, 650, 800, 1,000, 1,250. For AQ curves, sample CO_2 was set to 390 ppm and data was logged after a minimum of 3 min at each light intensity, using the following sequence of light intensities: 1,500, 1,000, 750, 500, 300, 200, 150, 50, 25, 10, 0. Reference and sample analyzers were matched prior to logging the data. Maximum Rubisco activity ($V_{c,max}$) and maximum electron transport rate used in RuBP regeneration (J_{max}) were fitted using the FvCB model and the Plantecophys package in R (Duursma 2015).

Thylakoid isolation

Thylakoids were isolated from Arabidopsis plants 2 to 3 h into the photoperiod. Plants were blended in ice-cold medium containing 50 mM sodium phosphate pH 7.4, 5 mM $MgCl_2$, 300 mM sucrose, and 10 mM NaF. The homogenate was then filtered twice through two layers of muslin cloth. The filtrate was then centrifuged for 15 min at 3750 × *g* at 4 °C. The chloroplast pellets were then resuspended in 5 mM $MgCl_2$, 10 mM Tricine pH 7.4, and 10 mM NaF. After 1 min on ice, a medium containing 5 mM MgCl2, 10 mM Tricine pH 7.4, 400 mM sucrose, and 10 mM NaF was added. The broken chloroplasts were centrifuged for 15 min at 3,750 × *g* at 4°C, and thylakoid pellets were resuspended in 10 mM sodium phosphate pH 7.4, 5 mM MgCl2, 5 mM NaCl, and 100 mM sucrose. Resuspended thylakoids were centrifuged again, and pellets were resuspended in 1 ml of the same medium.

Quantitative proteomic analysis of thylakoid membranes

Thylakoid membrane proteins were solubilized and digested with a combination of endoproteinase Lys-C and trypsin in 1% (w/v) sodium laurate, 100 mM triethylammonium bicarbonate pH 8.5 with additional sample processing and analysis by nano-flow liquid chromatography–mass spectrometry as previously described (Flannery et al. 2021). MaxQuant v. 1.6.3.4 (Cox and Mann 2008) was used for mass spectral data processing and protein identification with the iBAQ (Schwanhäusser et al. 2011) label-free quantification option selected and other parameters as previously specified (Flannery et al. 2021). iBAQ abundance scores subjected to statistical analysis using a modified Welch's *t*-test as implemented in Perseus v. 1.6.2.3 Protein identification and label-free quantification were performed using the MaxLFQ algorithm embedded within FragPipe (v. 16.0) (Yu et al. 2021). The "match-between-runs' option was selected and all other parameters were as per default. Total intensities were normalized against the sum of all identified proteins. Not all proteins were identified by mass spectrometry, therefore only proteins where >75% of replicates were identified were selected. The normal distribution of data was verified in MaxQuant (Cox and Mann 2008), imputed and $\log_2$ transformed. This data was then expressed as fold-change relative to wild type, where $P < 0.05$ was significantly different. The proteomics data have been deposited to the ProteomeXchange Consortium via the PRIDE partner repository (http://proteomecentral.proteomexchange.org) with the dataset identifier PXD033007.

Statistical analysis

Statistical analysis was performed using Graphpad Prism, 9.1.1, using a two-sided *t*-test (alpha = 0.05) and the Tukey HSD test (alpha = 0.05) in R. The asterisks always indicate significant differences between the Col-0 & *hope2* and *gl1* & *pgr5* or light treatments. Different letters indicate significant differences.

Accession numbers

Sequence data from this article can be found in the GenBank/EMBL data libraries under accession numbers AJ245502 (hope2/ATPC1), AY060546 (PGR5), BT000905 (PGRL1), AY143808 (NDHO).

Acknowledgments

We would like to thank Prof. Toshiharu Shikanai for the gift of *pgr5* seeds, Prof. Chikahiro Miyake for the gift of *hope2* seeds and Prof. Eva-Mari Aro for *ndho* seeds. For the purpose of open access, the author has applied a Creative Commons Attribution (CC BY) license to any Author Accepted Manuscript version arising.

Author contributions

G.E.D., M.S.P., P.J.J., and N.Z. performed the research; S.A.C. and M.P.J. supervised the research; G.E.D. analyzed the data, and G.E.D. and M.P.J. wrote the paper. All authors approved of the manuscript prior to submission.

Supplemental data

The following materials are available in the online version of this article.

Supplemental Figure S1. Abundance of photosynthetic proteins.

Supplemental Figure S2. Determination of PSI antenna size in Col-0 and *hope2*.

Supplemental Figure S3. Verification of homozygosity of double crosses.

Supplemental Figure S4. Growth of genotypes under control and high light conditions.

Supplemental Figure S5. Determination of rapidly relaxing NPQ (qE).

Supplemental Figure S6. Sequence alignment of Rossmann-fold from various organisms and organelles.

Funding

M.P.J. and S.A.C. acknowledge funding from the Leverhulme Trust grant RPG-2019-045.

Conflict of interest statement. None declared.

Data availability

The datasets analysed during the current study are available from the corresponding author on reasonable request.

References

Alric J, Johnson X. Alternative electron transport pathways in photosynthesis: a confluence of regulation. Curr Opin Plant Biol. 2017:**37**: 78–86

Armbruster U, Galvis VC, Kunz H-H, Strand DD. The regulation of the chloroplast proton motive force plays a key role for photosynthesis in fluctuating light. Curr Opin Plant Biol. 2017:**37**:56-62

Avenson TJ, Cruz JA, Kanazawa A, Kramer DM. Regulating the proton budget of higher plant photosynthesis. Proc Natl Acad Sci U S A. 2005:**102**(27):9709–9713

Baker NR, Harbinson J, Kramer DM. Determining the limitations and regulation of photosynthetic energy transduction in leaves. Plant Cell Environ. 2007:**30**(9):1107–1125

Busch FA. Photosynthetic gas exchange in land plants at the leaf level. Photosynth Methods Mol Biol. 2018:**1770**:25–44

Carrillo LR, Froehlich JE, Cruz JA, Savage LJ, Kramer DM. Multi-level regulation of the chloroplast ATP synthase: the chloroplast NADPH thioredoxin reductase C (NTRC) is required for redox modulation specifically under low irradiance. Plant J. 2016:**87**(6):654–663

Clark RD, Hawkesford MJ, Coughlan SJ, Bennett J, Hind G. Association of ferredoxin-$NADP^+$ oxidoreductase with the chloroplast cytochrome *b-f* complex. Febs Lett. 1984:**174**(1):137–142

Cox J, Mann M. Maxquant enables high peptide identification rates, individualized p.p.b.-range mass accuracies and proteome-wide protein quantification. Nat Biotechnol. 2008:**26**(12):1367–1372

DalCorso G, Pesaresi P, Masiero S, Aseeva E, Schünemann D, Finazzi G, Joliot P, Barbato R, Leister D. A complex containing PGRL1 and PGR5 is involved in the switch between linear and cyclic electron flow in Arabidopsis. Cell. 2008:**132**(2):273–285

Davis GA, Kanazawa A, Schöttler MA, Kohzuma K, Froehlich JE, Rutherford AW, Satoh-Cruz M, Minhas D, Tietz S, Dhingra A, et al. Limitations to photosynthesis by proton motive force-induced photosystem II photodamage. Elife. 2016:**5**:e16921. https://doi.org/10.7554/eLife.16921

Dobrescu A, Scorza LCT, Tsaftaris SA, McCormick AJ. A "do-it-yourself" phenotyping system: measuring growth and morphology throughout the diel cycle in rosette shaped plants. Plant Methods. 2017:**13**(1):95

Duursma RA. Plantecophys - an R package for analysing and modelling leaf gas exchange data. PLOS One. 2015:**10**(11):e0143346

Farquhar GD, von Caemmerer S, Berry JA. A biochemical model of photosynthetic CO2 assimilation in leaves of C3 species. Planta. 1980:**149**(1):78–90

Flannery SE, Hepworth C, Wood WHJ, Pastorelli F, Hunter CN, Dickman MJ, Jackson PJ, Johnson MP. Developmental acclimation of the thylakoid proteome to light intensity in *Arabidopsis*. Plant J. 2021:**105**(1):223–244

Hahn A, Vonck J, Mills DJ, Meier T, Kühlbrandt W. Structure, mechanism, and regulation of the chloroplast ATP synthase. Science **360**(6389):1-82018

Hald S, Nandha B, Gallois P, Johnson GN. Feedback regulation of photosynthetic electron transport by NADP(H) redox poise. Biochim Biophys Acta. 2008:**1777**(5):433–440

Hepworth C, Wood WHJ, Emrich-Mills TZ, Proctor MS, Casson S, Johnson MP. Dynamic thylakoid stacking and state transitions work synergistically to avoid acceptor-side limitation of photosystem I. Nat Plants. 2021:**7**:87–98

Hertle AP, Blunder T, Wunder T, Pesaresi P, Pribil M, Armbruster U, Leister D. PGRL1 Is the elusive ferredoxin-plastoquinone reductase in photosynthetic cyclic electron flow. Mol Cell. 2013:**49**(3):511–523

Hind G, Nakatani HY, Izawa S. Light-dependent redistribution of ions in suspensions of chloroplast thylakoid membranes. Proc Natl Acad Sci USA. 1974:**71**(4):1484–1488

Hisabori T, Ueoka-Nakanishi H, Konno H, Koyama F. Molecular evolution of the modulator of chloroplast ATP synthase: origin of the conformational change dependent regulation. Febs Lett. 2003:**545**(1):71–75

Horton P, Ruban AV, Rees D, Pascal AA, Noctor G, Young AJ. Control of the light-harvesting function of chloroplast membranes by aggregation of the LHCII chlorophyll—protein complex. Febs Lett. 1991:**292**(1–2):1–4

Jahns P, Graf M, Munekage Y, Shikanai T. Single point mutation in the Rieske iron–sulfur subunit of cytochrome b_6/f leads to an altered pH dependence of plastoquinol oxidation in *Arabidopsis*. Febs Lett. 2002:**519**(1–3):99–102

Johnson GN. Thiol regulation of the thylakoid electron transport ChainA missing link in the regulation of photosynthesis? Biochemistry-us. 2003:**42**(10):3040–3044

Johnson GN. Physiology of PSI cyclic electron transport in higher plants. Biochim Biophys Acta. 2011:**1807**(3):384–389

Joliot P, Béal D, Joliot A. Cyclic electron flow under saturating excitation of dark-adapted Arabidopsis leaves. Biochim Biophys Acta. 2004:**1656**(2–3):166–176

Joliot P, Johnson GN. Regulation of cyclic and linear electron flow in higher plants. Proc Natl Acad Sci USA. 2011:**108**(32):13317–13322

Joliot P, Joliot A. Cyclic electron transfer in plant leaf. Proc Natl Acad Sci USA. 2002:**99**(15):10209–10214

Junesch U, Gräber P. Influence of the redox state and the activation of the chloroplast ATP synthase on proton-transport-coupled ATP synthesis/hydrolysis. Biochim Biophys Acta. 1987:**893**(2): 275–288

Kanazawa A, Kramer DM. *In vivo* modulation of nonphotochemical exciton quenching (NPQ) by regulation of the chloroplast ATP synthase. Proc Natl Acad Sci USA. 2002:**99**(20):12789–12794

Klughammer C, Schreiber U. Deconvolution of ferredoxin, plastocyanin, and P700 transmittance changes in intact leaves with a new type of kinetic LED array spectrophotometer. Photosyn Res. 2016:**128**: 195–214

Klughammer C, Siebke K, Schreiber U. Continuous ECS-indicated recording of the proton-motive charge flux in leaves. Photosyn Res. 2013:**117**:471–487

Kohzuma K, Bosco CD, Kanazawa A, Dhingra A, Nitschke W, Meurer J, Kramer DM. Thioredoxin-insensitive plastid ATP synthase that performs moonlighting functions. Proc Natl Acad Sci USA. 2012:**109**(9):3293–3298

Kohzuma K, Bosco CD, Meurer J, Kramer DM. Light- and metabolism-related regulation of the chloroplast ATP synthase has distinct mechanisms and functions. J Biol Chem. 2013:**288**(18):13156–13163

Konno H, Nakane T, Yoshida M, Ueoka-Nakanishi H, Hara S, Hisabori T. Thiol modulation of the chloroplast ATP synthase is dependent on the energization of thylakoid membranes. Plant Cell Physiol. 2012:**53**(4):626–634

Kramer DM, Avenson TJ, Edwards GE. Dynamic flexibility in the light reactions of photosynthesis governed by both electron and proton transfer reactions. Trends Plant Sci. 2004:**9**(7):349–357

Kramer DM, Evans JR. The importance of energy balance in improving photosynthetic productivity. Plant Physiol. 2011:**155**(1):70–78

Kramer M, Rodriguez-Heredia M, Saccon F, Mosebach L, Twachtmann M, Krieger-Liszkay A, Duffy C, Knell RJ, Finazzi G, Hanke GT. Regulation of photosynthetic electron flow on dark to light transition by ferredoxin:nADP(H) oxidoreductase interactions. Elife. 2021:**10**:e56088. https://doi.org/10.7554/eLife.56088

Li Y, Ma X, Weber J. Interaction between γC87 and γR242 residues participates in energy coupling between catalysis and proton translocation in Escherichia coli ATP synthase. Biochim Biophys Acta. 2019:**1860**(8):679–687

Li Z, Wakao S, Fischer BB, Niyogi KK. Sensing and responding to excess light. Annu Rev Plant Biol. 2009:**60**(1):239–260

Livingston AK, Cruz JA, Kohzuma K, Dhingra A, Kramer DM. An *Arabidopsis* mutant with high cyclic electron flow around photosystem I (*hcef*) involving the NADPH dehydrogenase Complex. Plant Cell Online. 2010a:**22**(1):221–233

Livingston AK, Kanazawa A, Cruz JA, Kramer DM. Regulation of cyclic electron flow in C3 plants: differential effects of limiting photosynthesis at ribulose-1,5-bisphosphate carboxylase/oxygenase and glyceraldehyde-3-phosphate dehydrogenase. Plant Cell Environ. 2010b:**33**(11):1779–1788

Malone LA, Proctor MS, Hitchcock A, Hunter CN, Johnson MP. Cytochrome b 6 f – orchestrator of photosynthetic electron transfer. Biochim Biophys Acta. 2021:**1862**(5):148380

Mills JD, Mitchell P. Modulation of coupling factor ATPase activity in intact chloroplasts. Reversal of thiol modulation in the dark. Biochim Biophys Acta. 1982:**679**(1):75–83

Miyake C. Alternative electron flows (water–water cycle and cyclic electron flow around PSI) in photosynthesis: molecular mechanisms and physiological functions. Plant Cell Physiol. 2010:**51**(12): 1951–1963

Munekage Y, Hashimoto M, Miyake C, Tomizawa K-I, Endo T, Tasaka M, Shikanai T. Cyclic electron flow around photosystem I is essential for photosynthesis. Nature. 2004:**429**(6991):579–582

Munekage Y, Hojo M, Meurer J, Endo T, Tasaka M, Shikanai T. PGR5 is involved in cyclic electron flow around photosystem I and is essential for photoprotection in Arabidopsis. Cell. 2002:**110**(3):361–371

Nikkanen L, Diaz MG, Toivola J, Tiwari A, Rintamäki E. Multilevel regulation of non-photochemical quenching and state transitions by chloroplast NADPH-dependent thioredoxin reductase. Physiol Plantarum. 2019:**166**(1):211–225

Nikkanen L, Toivola J, Trotta A, Diaz MG, Tikkanen M, Aro E, Rintamäki E. Regulation of cyclic electron flow by chloroplast NADPH-dependent thioredoxin system. Plant Direct. 2018:**2**(11): e00093

Nishikawa Y, Yamamoto H, Okegawa Y, Wada S, Sato N, Taira Y, Sugimoto K, Makino A, Shikanai T. PGR5-dependent cyclic electron transport around PSI contributes to the redox homeostasis in chloroplasts rather than CO2 fixation and biomass production in rice. Plant Cell Physiol. 2012:**53**(12):2117–2126

Nishio JN, Whitmarsh J. Dissipation of the proton electrochemical potential in intact chloroplasts (II. The pH gradient monitored by cytochrome f reduction kinetics). Plant Physiol. 1993:**101**(1):89–96

Ojeda V, Pérez-Ruiz JM, Cejudo FJ. 2-Cys peroxiredoxins participate in the oxidation of chloroplast enzymes in the dark. Mol Plant. 2018:**11**-(11):1377–1388

Okegawa Y, Long TA, Iwano M, Takayama S, Kobayashi Y, Covert SF, Shikanai T. A balanced PGR5 level is required for chloroplast development and Optimum operation of cyclic electron transport around photosystem I. Plant Cell Physiol. 2007:**48**(10):1462–1471

Okegawa Y, Tsuyama M, Kobayashi Y, Shikanai T. The pgr1 mutation in the rieske subunit of the cytochrome b_6f complex does not affect PGR5-dependent cyclic electron transport around photosystem I. J Biol Chem. 2005:**280**(31):28332–28336

Ort DR, Oxborough K. In situ regulation of chloroplast coupling factor activity. Annu Rev Plant Phys. 1992:**43**(1):269–291

Penzler J-F, Marino G, Reiter B, Kleine T, Naranjo B, Leister D. Commonalities and specialties in photosynthetic functions of PROTON GRADIENT REGULATION5 variants in Arabidopsis. Plant Physiol. 2022:**190**(3):1866–1882

Rantala S, Lempiäinen T, Gerotto C, Tiwari A, Aro E-M, Tikkanen M. PGR5 And NDH-1 systems do not function as protective electron acceptors but mitigate the consequences of PSI inhibition. Biochim Biophys Acta. 2020:**1861**(3):148154

Rees D, Young A, Noctor G, Britton G, Horton P. Enhancement of the ΔpH-dependent dissipation of excitation energy in spinach chloroplasts by light-activation:correlation with the synthesis of zeaxanthin. Febs Lett. 1989:**256**(1–2):85–90

Rott M, Martins NF, Thiele W, Lein W, Bock R, Kramer DM, Schöttler MA. ATP synthase repression in tobacco restricts photosynthetic electron transport, CO_2 assimilation, and plant growth by overacidification of the thylakoid lumen. Plant Cell. 2011:**23**(1): 304–321

Ruban AV, Johnson MP, Duffy CDP. The photoprotective molecular switch in the photosystem II antenna. Biochim Biophys Acta. 2012:**1817**(1):167–181

Rühle T, Dann M, Reiter B, Schünemann D, Naranjo B, Penzler J-F, Kleine T, Leister D. PGRL2 triggers degradation of PGR5 in the absence of PGRL1. Nat Commun. 2021:**12**(1):3941

Rumeau D, Bécuwe-Linka N, Beyly A, Louwagie M, Garin J, Peltier G. New subunits NDH-M, -N, and -O, encoded by nuclear genes, are essential for plastid Ndh complex functioning in higher plants. Plant Cell. 2005:**17**(1):219–232

Schreiber U, Klughammer C (2016) Analysis of photosystem I donor and acceptor sides with a new type of online-deconvoluting kinetic LED-array spectrophotometer. Plant and Cell Physiology **57**(7): 1454-1467

Schwanhäusser B, Busse D, Li N, Dittmar G, Schuchhardt J, Wolf J, Chen W, Selbach M. Global quantification of mammalian gene expression control. Nature. 2011:**473**(7347):337–342

Sekiguchi T, Yoshida K, Okegawa Y, Motohashi K, Wakabayashi K, Hisabori T. Chloroplast ATP synthase is reduced by both f-type and m-type thioredoxins. Biochim Biophys Acta. 2020:**1861**(11): 148261

Shahak Y, Crowther D, Hind G. The involvement of ferredoxin-NADP + reductase in cyclic electron transport in chloroplasts. Biochim Biophys Acta. 1981:**636**(2):234–243

Shen L, Tang K, Wang W, Wang C, Wu H, Mao Z, An S, Chang S, Kuang T, Shen J-R, et al. Architecture of the chloroplast PSI–NDH supercomplex in Hordeum vulgare. Nature. 2022:**601**(7894):649–654

Strand DD, Fisher N, Davis GA, Kramer DM. Redox regulation of the antimycin A sensitive pathway of cyclic electron flow around photosystem I in higher plant thylakoids. Biochim Biophys Acta. 2016:**1857**(1):1–6

Strand DD, Livingston AK, Satoh-Cruz M, Froehlich JE, Maurino VG, Kramer DM. Activation of cyclic electron flow by hydrogen peroxide in vivo. Proc Natl Acad Sci USA. 2015:**112**(17):5539–5544

Strand DD, Livingston AK, Satoh-Cruz M, Koepke T, Enlow HM, Fisher N, Froehlich JE, Cruz JA, Minhas D, Hixson KK, et al. Defects in the expression of chloroplast proteins leads to H2O2 accumulation and activation of cyclic electron flow around photosystem I. Front Plant Sci. 2017:**7**:2073

Su X, Cao D, Pan X, Shi L, Liu Z, Dall'Osto L, Bassi R, Zhang X, Li M. Supramolecular assembly of chloroplast NADH dehydrogenase-like complex with photosystem I from Arabidopsis thaliana. Mol Plant. 2022:**15**(3):454–467

Suorsa M, Grieco M, Järvi S, Gollan PJ, Kangasjärvi S, Tikkanen M, Aro E-M. PGR5 Ensures photosynthetic control to safeguard photosystem I under fluctuating light conditions. Plant Signal Behav. 2013:**8**(1):e22741

Suorsa M, Järvi S, Grieco M, Nurmi M, Pietrzykowska M, Rantala M, Kangasjärvi S, Paakkarinen V, Tikkanen M, Jansson S, et al. PROTON GRADIENT REGULATION5 is essential for proper acclimation of *Arabidopsis* photosystem I to naturally and artificially fluctuating light conditions. Plant Cell Online. 2012:**24**(7):2934–2948

Takagi D, Amako K, Hashiguchi M, Fukaki H, Ishizaki K, Goh T, Fukao Y, Sano R, Kurata T, Demura T, et al. Chloroplastic ATP synthase builds up a proton motive force preventing production of reactive oxygen species in photosystem I. Plant J. 2017:**91**(2):306–324

Takagi D, Miyake C. PROTON GRADIENT REGULATION 5 supports linear electron flow to oxidize photosystem I. Physiol Plantarum. 2018:**164**(3):337–348

Takizawa K, Cruz JA, Kanazawa A, Kramer DM. The thylakoid proton motive force in vivo. Quantitative, non-invasive probes, energetics, and regulatory consequences of light-induced pmf. Biochim Biophys Acta. 2007:**1767**(10):1233–1244

Takizawa K, Kanazawa A, Kramer DM. Depletion of stromal pi induces high 'energy-dependent' antenna exciton quenching (qE) by decreasing proton conductivity at CFO-CF1 ATP synthase. Plant Cell Environ. 2008:**31**(2):235–243

Velthuys BR. A third site of proton translocation in green plant photosynthetic electron transport. Proc Natl Acad Sci USA. 1978:**75**(12):6031–6034

Wada S, Amako K, Miyake C. Identification of a novel mutation exacerbated the PSI photoinhibition in pgr5/pgrl1 mutants; caution for overestimation of the phenotypes in Arabidopsis pgr5-1 mutant. Cells. 2021:**10**(11):2884

Wang C, Takahashi H, Shikanai T. PROTON GRADIENT REGULATION 5 contributes to ferredoxin-dependent cyclic phosphorylation in ruptured chloroplasts. Biochim Biophys Acta. 2018:**1859**(10):1173–1179

Wang C, Yamamoto H, Shikanai T. Role of cyclic electron transport around photosystem I in regulating proton motive force. Biochim Biophys Acta. 2015:**1847**(9):931–938

Wilson S, Johnson MP, Ruban AV. Proton motive force in plant photosynthesis dominated by ΔpH in both low and high light. Plant Physiol. 2021:**187**(1):263–275

Yamamoto H, Shikanai T. Does the Arabidopsis *proton gradient regulation 5* mutant leak protons from the thylakoid membrane? Plant Physiol. 2020:**184**(1):421

Yamamoto H, Takahashi S, Badger MR, Shikanai T. Artificial remodelling of alternative electron flow by flavodiiron proteins in Arabidopsis. Nat Plants. 2016:**2**(3):16012

Yamori W, Makino A, Shikanai T. A physiological role of cyclic electron transport around photosystem I in sustaining photosynthesis under fluctuating light in rice. Sci Rep. 2016:**6**(1):20147

Yamori W, Sakata N, Suzuki Y, Shikanai T, Makino A. Cyclic electron flow around photosystem I via chloroplast NAD(P)H dehydrogenase (NDH) complex performs a significant physiological role during photosynthesis and plant growth at low temperature in rice. Plant J. 2011:**68**(6):966–976

Yamori W, Shikanai T. Physiological functions of cyclic electron transport around photosystem I in sustaining photosynthesis and plant growth. Annu Rev Plant Biol. 2015:**67**:1–26

Yamori W, Shikanai T, Makino A. Photosystem I cyclic electron flow via chloroplast NADH dehydrogenase-like complex performs a physiological role for photosynthesis at low light. Sci Rep. 2015:**5**(1):13908

Yu F, Haynes SE, Nesvizhskii AI. IonQuant enables accurate and sensitive label-free quantification with FDR-controlled match-between-runs. Mol Cell Proteomics. 2021:**20**:100077

Zhang H, Whitelegge JP, Cramer WA. Ferredoxin:NADP+ oxidoreductase is a subunit of the chloroplast cytochrome b6fComplex. J Biol Chem. 2001:**276**(41):38159–38165

Zhou Q, Wang C, Yamamoto H, Shikanai T. PTOX-dependent safety valve does not oxidize P700 during photosynthetic induction in the Arabidopsis *pgr5* mutant. Plant Physiol. 2022:**188**(2):1264–1276